

Requirements for very high temperature Kohn-Sham density functional simulations and how to bypass them

A. Blanchet,^{1,2} M. Torrent,^{1,2} and J. Clérouin^{1,2}

¹⁾*CEA-DAM-DIF, F-91297 Arpajon, France*

²⁾*Université Paris-Saclay, CEA, Laboratoire Matière en Conditions Extrêmes, 91680 Bruyères-le-Châtel, France*

(Dated: 25 August 2020)

In density functional high temperature simulations (from tens of eV to keV) the total number of Kohn-Sham orbitals is a critical quantity to get sound results. The occupation of the highest orbital in energy is here derived from the properties of the homogeneous electron gas, which gives a prescription on the total number of orbitals to reach a given level of occupation. Very low levels of occupation (10^{-5} - 10^{-6}) must be considered to get convergence with Kohn-Sham orbitals, making high temperature simulations unreachable beyond a few tens of eV. After testing these predictions against ABINIT software package results, we test the implementation of the Extended method of Zhang *et al.* [PoP **23** 042707, 2016] in the ABINIT package to address very high temperatures by bypassing these strong orbital constraint.

I. INTRODUCTION

Kohn-Sham density functional theory (KSDFT) simulations are now a well established technique to compute properties of matter at ambient conditions with a large number of available computer codes. Among them, the ABINIT¹⁻³ software package provides the largest variety of pseudo-potentials, exchange-correlation functionals and intensive parallelization in a open-source environnement.

The extension of this technique towards disordered hot systems was historically introduced in codes such as VASP⁴, through the Mermin finite temperature functional⁵. This approach, well adapted up to a few eV, which corresponds to the domain of liquid metals⁶, becomes prohibitively expensive at higher temperatures (tens of eV), entering the warm dense matter regime (WDM). In this regime, KSDFT simulations are quickly unable to cope with the huge number of quasi empty orbitals necessary to insure convergence. This is a critical point we are going to develop later.

On the other hand, techniques based on path-integral Monte-Carlo (PIMC)^{7,8}, or on the density matrix, have been developed that provide a nearly exact solution at high temperature (at the node approximation), but are increasingly slower and prohibitively expensive at low temperature.

A simplified approach has been proposed, using an orbital-free (OFDFT) formulation at high temperature, bypassing the quantum expression of the electronic kinetic energy with orbitals by a semi-classical finite temperature Thomas-Fermi formulation^{9,10}. This method is very fast for temperatures beyond tens of eVs, but yields poor results below. The transition from the KSDFT formulation at low temperature to the OFDFT, as the temperature rises, was described very early¹¹, and solutions have been proposed using the bootstrap method¹² to compute hugoniots or by introducing a KSDFT reference points¹³ for building a coherent equation of state.

More recently, Zhang *et al.*¹⁴ proposed to combine the two techniques into the so-called Extended method, by replacing high energy orbitals by plane waves, allowing for a continuous transition from cold materials to hot plasmas.

A systematic comparison of those different approaches has

been done recently during a blind comparison workshop¹⁵.

In this paper we propose to provide a quantitative prescriptions for high temperature KSDFT simulations. After discussing an example illustrating of the convergence of the pressure with the number of orbitals involved in the calculation, we introduce a simple model based on the homogeneous electron gas (HEG) to predict the number of orbitals required to fulfil a given occupancy. Then, we compare these predictions with ABINIT minimizations and we apply these requirements to analyze previous hydrogen and aluminum molecular dynamics simulations at very high temperature. To bypass the convergence constraints, we discuss the recently introduced Extended method, and we show, through its implementation in the ABINIT software package, how very high temperature simulations are easily performed and with the same level of accuracy than PIMC calculations.

II. CONVERGENCE WITH ORBITALS

We show in Fig. 1 (a) the electronic pressure of aluminum computed at a temperature of 20 eV, with an increasing number of orbitals. One can see that a minimum of 128 orbitals per atom is needed to get a precision of about 2% (see numbers in Table I), when at low temperature, for 11 valence electrons, six doubly occupied orbitals¹⁶, are enough. The increase from 6 to 128 orbitals per atom represents a computational effort about 20^3 higher. At high temperature we are facing up a paradoxal situation where a large number of slightly filled orbitals must be included with a computational cost proportional to the cube of this number (orthogonalization constraint). Very often, for KSDFT calculations in the WDM regime, this condition is even not mentioned and the number of orbitals evaluated *au petit bonheur*.

The accuracy of the pressure estimation depends on the number of orbitals, because, as soon as the electronic temperature is non-zero, the distribution of the electronic orbitals is no longer bounded and goes *stricto sensu* to infinity. In simulations, involving a finite number of orbitals, the last orbital in energy has a certain level of occupancy, that we will call

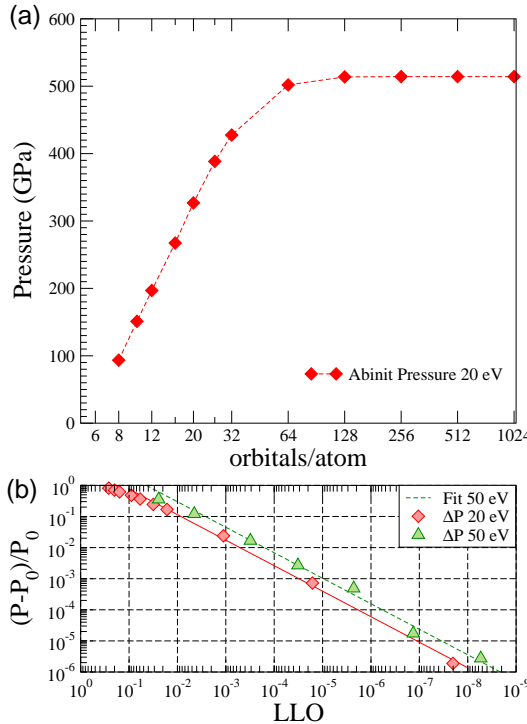


FIG. 1. (Color online) (a) Convergence of the electronic pressure versus the number of orbitals per atom for a 4 aluminum atoms system at 20 eV and normal density ρ_0 (red diamonds). (b) Relative accuracy of the pressure calculation $\Delta P = (P - P_0)/P_0$ versus LLO, where P_0 is the pressure given by the highest number of orbitals (see Table I). Red diamonds are for 20 eV data, and green up triangles for 50 eV. Corresponding straight lines are least squares fits. Note that the abscissa scale is reversed.

the last level occupancy (LLO). The first condition for doing sound simulations is to ensure that the LLO is low enough to give converged quantities. As shown in a recent study of MgO in the warm dense regime¹⁷, a LLO of 10^{-5} is necessary to converge the pressure better than 0.1%. We show in Fig. 1 (b), the convergence of the relative error on the electronic pressure $\Delta P/P_0 = (P - P_0)/P_0$, where P_0 is the converged pressure, versus LLO (see also Table I, columns 1; 2 and 5, for 20 eV data). One can see that to get 1% precision, a LLO between 10^{-3} and 10^{-4} is needed, and to go below 1%, a LLO between 10^{-4} and 10^{-5} must be considered.

An empirical relation between the relative error and the LLO α is, $\Delta P/P_0 = 5\alpha^{0.82}$ for 20 eV data (red diamonds and straight red line), and $\Delta P/P_0 = 13\alpha^{0.82}$ for 50 eV data (green up triangles and dashed green line). These empirical rules, that seem weakly dependant on the temperature, give the good order of magnitude of the precision of the calculation versus the last orbital occupation (LLO).

III. HOMOGENEOUS ELECTRON GAS MODEL

The occupancy of electronic states being given by the Fermi-Dirac statistics, the fundamental parameter for high

TABLE I. Finite temperature evaluation of the electronic pressure of four aluminum atom at normal density and at 20 eV and for a varying number of orbitals. The PAW pseudo-potential involves 11 electrons.

Bands /atom	LLO	Pressure GPa	corrected GPa	error %	corrected %
8	$2.6 \cdot 10^{-1}$	93.49901	461.85606	$8.2 \cdot 10^{-1}$	$1.0 \cdot 10^{-1}$
10	$2.0 \cdot 10^{-1}$	151.10035	495.28772	$7.1 \cdot 10^{-1}$	$3.7 \cdot 10^{-2}$
12	$1.6 \cdot 10^{-1}$	196.87071	524.37561	$6.2 \cdot 10^{-1}$	$1.9 \cdot 10^{-2}$
16	$8.9 \cdot 10^{-2}$	267.26940	487.05498	$4.8 \cdot 10^{-1}$	$5.3 \cdot 10^{-2}$
20	$5.9 \cdot 10^{-2}$	326.88243	528.86232	$3.6 \cdot 10^{-1}$	$2.8 \cdot 10^{-2}$
26	$3.2 \cdot 10^{-2}$	388.38812	513.03870	$2.4 \cdot 10^{-1}$	$2.3 \cdot 10^{-3}$
32	$1.6 \cdot 10^{-2}$	427.61530	506.51376	$1.7 \cdot 10^{-1}$	$1.5 \cdot 10^{-2}$
64	$1.1 \cdot 10^{-3}$	501.95302	513.50306	$2.4 \cdot 10^{-2}$	$1.4 \cdot 10^{-3}$
128	$1.6 \cdot 10^{-5}$	513.83618	514.17545	$7.2 \cdot 10^{-4}$	$6.3 \cdot 10^{-5}$
256	$2.0 \cdot 10^{-8}$	514.20696	514.20787	$1.9 \cdot 10^{-6}$	$1.2 \cdot 10^{-7}$
512	$3.5 \cdot 10^{-13}$	514.20793	514.20793	0.	0.
1024	$1.0 \cdot 10^{-15}$	514.20793	514.20793	0.	0.

temperature KSDFT simulations is not the temperature itself, but rather the Fermi degeneracy defined by $\theta = k_B T / \epsilon_F$.

For a HEG, the Fermi energy ϵ_F , expressed in atomic units $e = m = \hbar = 1$ reads

$$\epsilon_F = k_B T_F = \left(\frac{2}{G} \right)^{2/3} \frac{(3\pi^2)^{2/3}}{2} n_V^{2/3}, \quad (1)$$

where $n_V = N_V / V_{at}$ is the the electronic density. V_{at} is the atomic volume, N_V is the number of valence electrons, and G the degeneracy of the electronic state.

In a KSDFT approach the valence electrons are defined as electrons not belonging to the frozen core of the pseudo-potential. These electrons can go to the continuum (ionization) and participate to the electronic density. Usually, for aluminum, the outermost three electrons ($3s^2 3p^1$) are counted in the valence states, which is enough up to a few eV. But if we want to go at much higher temperatures, 11 electrons ($2s^2 2p^6 3s^2 3p^1$) must be considered, leaving the very deep $1s^2$ states in the core. To reach extreme conditions, an all electron description is necessary.

The number of orbitals fulfilling a given LLO α can be estimated from the HEG properties. In the following, we use the Fermi-Dirac distribution with a G degenerate occupancy as in the ABINIT software package

$$f(\epsilon) = \frac{G}{e^{\beta(\epsilon - \mu)} + 1}, \quad (2)$$

where $\beta = 1/k_B T$, ϵ the energy and μ the chemical potential.

The energy for which the Fermi-Dirac distribution is equal to α is

$$E_\alpha^* = \theta \ln \left[\frac{G}{\alpha} - 1 \right] + \mu^*, \quad (3)$$

where we have introduced the dimensionless quantities $\mu^* = \mu / \epsilon_F$ and $E_\alpha^* = E_\alpha / \epsilon_F$. $\alpha = 10^{-2}, 10^{-3}, \dots, 10^{-6}$ is the level of requested occupation of the last orbital.

The chemical potential of the HEG, obtained by comparing the number of particles at zero temperature with its expression at finite temperature¹⁸, reads

$$\mu^* = \theta I_{1/2}^{-1}[y], \quad (4)$$

where $y = \frac{2}{3}\theta^{-3/2}$. In this expression, $I_{1/2}^{-1}$ is the inverse of the Fermi integral of order 1/2. The chemical potential is equal to the Fermi energy at zero temperature, is zero for $\theta = 1$ and turns more and more negative beyond.

The number of quantum states per atom is

$$\begin{aligned} N^* &= \frac{G}{2} \frac{2^{3/2}}{3\pi^2} V \epsilon^{3/2} \quad (5) \\ &= \frac{G}{2} \frac{2^{3/2}}{3\pi^2} V \epsilon_F^{3/2} (\epsilon/\epsilon_F)^{3/2} \\ &= N_V \epsilon^{*3/2}. \end{aligned}$$

The number of orbitals, degenerate G times is thus

$$N_o = N_V / G * \epsilon^{*3/2}. \quad (6)$$

By expliciting Eq. (3) we obtain the number of doubly occupied states ($G=2$) per atom

$$N_o = \theta^{3/2} \left(\ln \left[\frac{2}{\alpha} - 1 \right] + I_{1/2}^{-1} \left[\frac{2}{3} \theta^{-3/2} \right] \right)^{3/2} \frac{N_V}{2}. \quad (7)$$

The total number of doubly occupied orbitals needed for a simulation of N_{at} atoms is $N_{\text{tot}} = N_o N_{\text{at}}$.

At high temperature $\beta \mu \approx \ln[y]$ and if we drop the 1 in the first logarithm we end up with the high temperature expression

$$N_o^{\text{HT}} \approx \theta^{3/2} \left(\ln \left[\frac{4}{3\alpha \theta^{3/2}} \right] \right)^{3/2} \frac{N_V}{2}. \quad (8)$$

This later expression predicts about 2-3% less orbitals at high temperature ($T \gtrsim T_F$) than the exact one but does not require to compute a Fermi integral. It must not be used below one tens of the Fermi temperature.

We have drawn in Fig. 2 (a) the number of doubly occupied orbitals versus reduced temperature corresponding to various LLOs from 10^{-6} (top black) to 10^{-1} (bottom indigo). There are many option for drawing the number of orbitals corresponding to a given LLO. Although the relations (7) and (8) are universal, we have chosen a particular case: aluminum with 11 valence electrons. At low temperature ($\theta \ll 1$), we can see that 6 doubly occupied are enough to satisfy any level of accuracy. This is no longer the case as soon as $\theta \simeq 0.1$ as shown in Fig. 2(b). When 8 orbitals (per atom) are enough to ensure a poor precision of 10^{-1} , 16 orbitals are necessary to reach a LLO of 10^{-4} . Those numbers are rapidly growing with temperature (as $T^{3/2}$), reaching very large values.

The constant LLO curves are non monotonic, but exhibit a maximum and then drop to zero. For each LLO, there is a maximum temperature θ_{max} beyond which a bijection between the number of orbitals and temperature can not be established. It can be obtained, with a good approximation, by

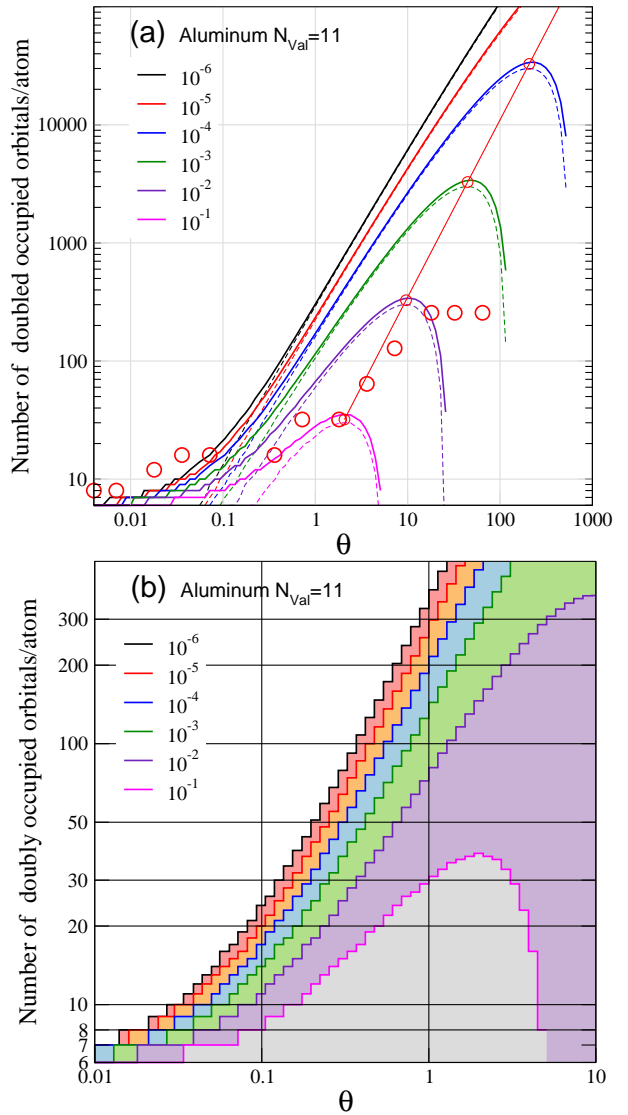


FIG. 2. (Color online) (a) Number of doubly occupied orbitals per aluminum atom ($N_V = 11$) versus degeneracy θ required to fulfil various LLO constrain from 10^{-6} (top black) to 10^{-1} (bottom indigo). Solid lines: exact calculation (7) and dashed lines: high temperature approximation (8). The solid line locate the corresponding maxima (red circles). (b): enlargement around $\theta = 1$.

taking the temperature derivative of Eq. (8) which gives

$$\theta_{\text{max}} = \frac{1}{e} \left(\frac{2G}{3\alpha} \right)^{2/3}, \quad (9)$$

where $e = 2.71838$ is the usual Neper number. Maxima correspond to the maximum doubly occupied orbitals per atom

$$N_{\alpha} = \frac{1}{e^{3/2}} \left(\frac{3}{2} \right)^{3/2} \frac{2G}{3\alpha}, \quad (10)$$

that are shown by open circles in Fig. 2. These maxima are connected by the relation $N_{\alpha} = (3/2)^{3/2} \theta^{3/2}$, solid red line in Fig. 2.

IV. CONNECTION WITH ORBITALS

In this section we assess the previous predictions by performing electronic minimizations using the ABINIT software package with an increasing number of orbitals at a given temperature.

A. Fermi energy

The HEG description relies upon a given electronic density n_V , which defines a Fermi energy. The chemical potential computed in ABINIT (improperly called Fermi level because it was originally designed for zero temperature calculations) does not correspond to our evaluation with 11 valence electrons. This is consequence of the pseudo-potential in use which shifts this quantity.

The connection with the HEG model is made by adding $\delta_E = \varepsilon_F^{\text{HEG}} - \varepsilon_F^{\text{ABINIT}}$ to the energies and to the chemical potential given by ABINIT. This convention give consistent results, as shown in Fig. 3(a), where the chemical potential given by ABINIT is compared with its HEG counterpart given by Eq. (4) along isochores of aluminum one, two, and five fold compressed. If at low temperature we get some variations, due to bounded states, at high temperature (Fig. 3(b)), we fit more and more closely the HEG relation (4).

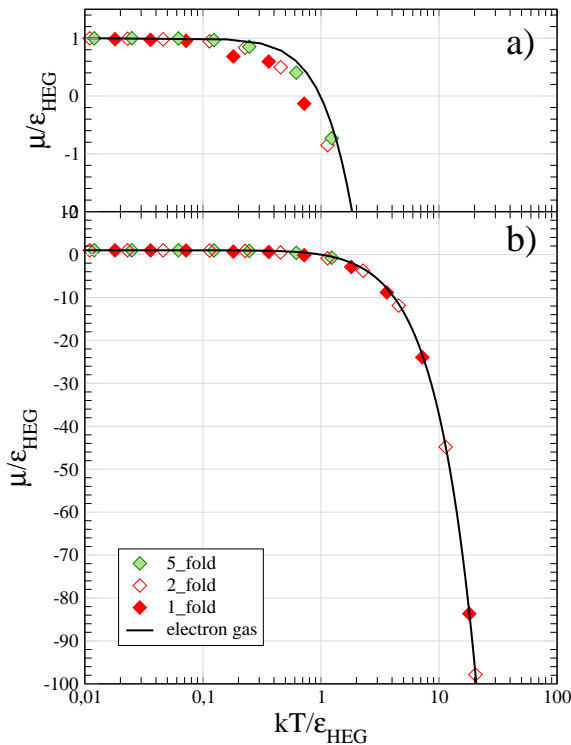


FIG. 3. ABINIT chemical potential (symbols) compared with HEG (solid lines) versus the HEG degeneracy $\theta = kT/\varepsilon_{\text{HEG}}$.

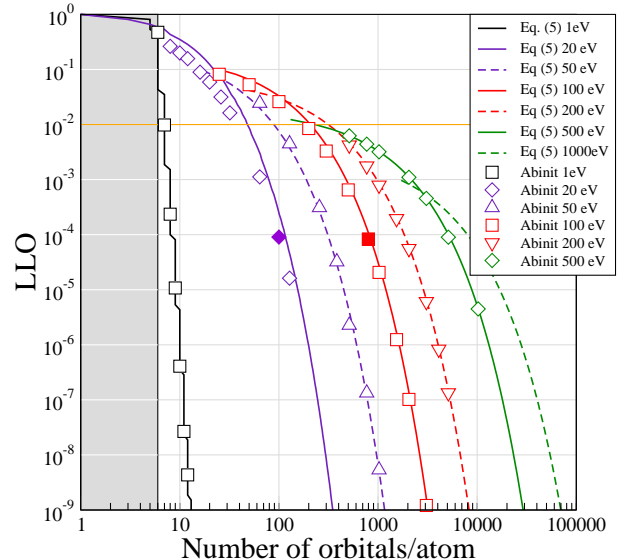


FIG. 4. (Color online) Last level occupation from ABINIT (symbols) compared with Eq. (7) (solid and dashed lines) for different temperatures from 0.001 to 1000 eV.

B. Occupations

Fig. 4 compares the LLO predicted by the HEG (Eq. (7), full and dotted lines) with the same quantity obtained from an ABINIT electronic minimization (symbols), with an increasing number of orbitals at a given temperature for a four aluminum atoms system. The agreement is very good in a wide range of high temperatures. The only difference is observed at low temperature (20 eV) where the HEG formula clearly overestimates the LLO obtained with ABINIT (blue diamonds).

C. Comparison with previous high temperature KSDFT simulations

These predictions are in good agreement with previous high temperature KSDFT calculations. The first one is a rather old simulation of of very dense hydrogen^{19,20}. In this case, the very high densities considered, representative of inertial confinement situations (80 and 160 g/cm³) allowed to successfully manage a large number of orbitals for 256 atoms up to 800 eV corresponding to an LLO between 10⁻⁶, necessary to obtain high quality optical properties. The number of orbitals predicted by our model are close to the one used (see Table II).

The second one, is a recent series of aluminum simulations, done by Driver²¹, under various compressions, for which the "low" temperature (0-100 eV) regime was computed with KSDFT simulations. In the worse case, at normal density, up to 76000 bands would be needed for a 64 atoms simulation at 100 eV, to comply with a LLO of 10⁻⁵, in agreement with the predictions of our model²². To reduce the computational load, 16 and 8 atoms were used at 100 eV and a LLO of 10⁻⁴ was preferred.

TABLE II. Number of orbitals predicted by Eq. (7) for a KSDFT simulation of 256 atoms hydrogen at 80 and 160 g/cm³ and temperatures of 172, 300 and 800 eV. The requested LLO is 10⁻⁶.

ρ g/cm ³	Fermi eV	T eV	θ	$N_o^{10^{-6}}$ model	N_o^{tot} 256
80	482	172	0.36	8	2048
80	482	300	0.62	15	3840
80	482	800	1.66	54	13824
160	765	172	0.22	5	1280
160	765	300	0.39	9	2304
160	765	800	1.05	30	7680

V. THE EXTENDED METHOD

A. Density of states

In our modelization, we have used the homogeneous electron gas to describe electron statistics. Doing that, we ignore the electronic structure and do not include bound states of negative energy. The density of states (DOS)²³, computed for aluminum at 20 eV with ABINIT, shown in Fig. 5, reveals bounded levels, at negative energies, merging with a continuum at high energy. This strongly suggests to break the calculations (density, energy, entropy) into two parts: a discrete part accounting for N_c discrete levels and a continuous part, using a continuous description with a DOS $g(\epsilon)$. For example, the kinetic energy reads

$$E = - \sum_{i=1}^{N_c} f(\epsilon_i) \langle \psi_i | \nabla^2 | \psi_i \rangle + \int_{E_C}^{\infty} f(\epsilon) g(\epsilon) \epsilon d\epsilon, \quad (11)$$

where N_c is the number of considered eigenstates states ψ_i with occupation f . The occupation $f(\epsilon_c)$ is nothing else than our previously introduced LLO.

B. Introduction of the homogeneous electron gas

Fig. 5 shows that the high energy part of the DOS identifies with the one of the homogeneous electron gas, shifted by an energy U_0

$$D(\epsilon) = \frac{\sqrt{2}\Omega}{\pi^2} \sqrt{\epsilon - U_0}, \quad (12)$$

where Ω is the volume. The agreement between the KSDFT DOS and the homogeneous electron gas is optimized by the choice of U_0 and by a proper average of the DOS either by including enough k -points or by considering large systems with many particles.

As U_0 is set and a cutoff energy E_c chosen we obtain the density

$$n(\mathbf{r}) = 2 \sum_{i=1}^{N_c} f(\epsilon_i) |\psi_i(\mathbf{r})|^2 - \frac{1}{\Omega} \int_{E_C}^{\infty} f(\epsilon) D(\epsilon) d\epsilon \quad (13)$$

$$= n(\mathbf{r})_{KS} + n_0, \quad (14)$$

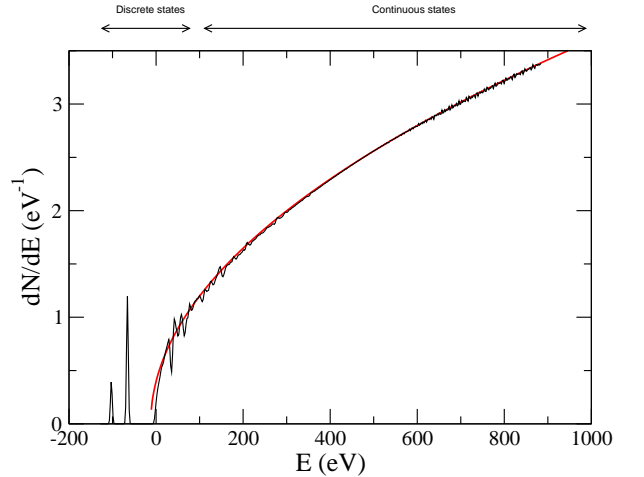


FIG. 5. (Color online) FCC Al DOS at 20 eV computed with 770 k -points. In red, the HEG density of states.

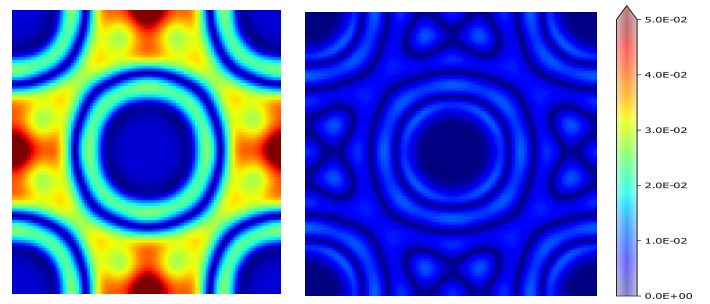


FIG. 6. (Color online) Relative errors in the density $\Delta n = (n(\mathbf{r})_{KS} - n(\mathbf{r})_{KS}^{Exact})/n(\mathbf{r})_{KS}^{Exact}$ for a 200 orbitals simulation. Left uncorrected, right corrected with the constant density n_0 .

The last term in Eq. (14) n_0 is a constant and is used to correct poorly converged Kohn-Sham densities. In other words, the Extended method uses high LLOs (10^{-3} to 10^{-2} instead of 10^{-5}) in KSDFT simulations to spare order of magnitude of computer time. This scheme allows for simulations up to a few keVs, corresponding to a very weak degeneracy ($\theta \gg 1$).

C. Precision

Returning to the previous calculation on aluminum at 20 eV and ρ_0 , we can see on Table I that a level of precision of 0.2% after correction is obtained with 128 orbitals/atom instead of 512 orbitals/atom.

It must be noted that this separation has two consequences. First, it allows to do the KSDFT part of the calculation with a high LLO, i.e. a low number of orbitals, which considerably reduces the computer time. Second, the HEG part, for all quantities of interest, is given by an analytical expressions. For example, the constant term n_0 of the density in Eq. (14) is

TABLE III. Total pressures obtained by the **Extended method**, along isochore ρ_0 . N_o is the prescription given by Eq. (7) corresponding to an LLO of 10^{-4} and N_o^{Ext} the number of orbitals used in the calculation. P_{Driver} is the interpolated Driver's pressures for our set of temperatures.

T eV	N_o/at Eq. (7)	$N_o^{\text{Ext}}/\text{at}$ Extended	N_{at}	P_{Ext} GPa	P_{Driver} GPa
ρ_0					
0.1	6	8	64	6.0	-
1	11	16	64	38.0	39.7
2	11	16	64	70.0	71.2
10	49	16	64	333	347
20	115	32	32	740	777
100	814	64	16	7365	7693
200	1837	128	16	19100	19400
500	5126	256	8	54000	59452
1000	10428	256	8	128850	130042
2000	19332	256	8	263900	266235

given by the expression

$$n_0 = -\frac{2\sqrt{2}}{\pi^2 \beta^{3/2}} I_{1/2}^c(\eta, x_c) \quad (15)$$

where $I_{1/2}^c(\eta, x_c)$ is the incomplete Fermi integral of index 1/2 of argument η and lower bound x_c . This integral, that can be exactly computed, is equivalent to an infinitely small LLO. Zhang *et al.*¹⁴ have shown that a non negligible part of the precision lies between 10^{-4} and 10^{-6} LLO.

As soon as the code is feed up with the new density $n(\mathbf{r})_{KS} + n_0$, the pressure and forces are defined straightforwardly, allowing for molecular dynamics simulations. Table I shows the efficiency of this correction with poorly converged pressures. The left and right panels of Fig. 6 display the error on the electronic density $\Delta n/n = (n(\mathbf{r})_{KS} - n(\mathbf{r})_{KS}^{\text{Exact}})/n(\mathbf{r})_{KS}^{\text{Exact}}$ for uncorrected (a) and corrected by the constant term n_0 of Eq. (14) (b).

D. Aluminum isochores

We consider now a disordered system of 64 atoms of aluminum from 0.1-fold to ten-fold compressed. Temperatures are ranging between 0.1 to 2 keV. The KSDFT part of the **Extended method** was realized with the ABINIT software package, with the projector augmented wave (PAW) method. Depending on the temperature, different atomic datas relatively to the electronic temperature were considered. From $T=0$ eV to $T=50$ eV, we used a PAW-LDA small core (11 valence electrons) pseudo-potential generated by N. A. W. Holzwarth with ATOMPAW software²⁴. From $T=50$ eV to $T=500$ eV, we used a PAW-LDA small core (11 valence electrons) pseudo-potential with small core radius, also used by K. P. Driver²¹ on his aluminum KSDFT/PIMC computations. The small core radius ($r_c = 0.6$ a.u.) ensures to limit PAW spheres overlapping during molecular dynamics at high temperatures. For temperatures higher than $T=500$ eV, an ultrasoft

all-electrons pseudo-potential generated by V. Recoules with ATOMPAW, was necessary.

The pressure is the sum of the electronic pressure and the ionic kinetic contribution. We compare in Fig. 7 the total pressure (symbols) with the data given in the supplemental of Driver's paper²¹ (straight lines), done with KSDFT simulations up to a temperature of 170 eV and with PIMC simulations beyond. The agreement with Driver's data, is excellent even up to 2000 eV (see columns 5 and 6 of Table III), which is impressive for a extended KSDFT method.

The settings of orbitals are shown in Table III. For each temperature, the second column gives the number of orbitals per atoms necessary to fulfil a given LLO of 10^{-4} (Eq. 7) compared with the number of orbitals we used with the **Extended method** (third column). Up to 2 eV these numbers are comparable due to the degeneracy. As the temperature rises the **Extended method** allows to keep only 64 orbitals per atoms instead of 814, and 256 instead of 19332 at 2 keV. Note that at this later temperature, a special full electrons pseudo-potential ($N_V = 13$) must be used. The number of atoms must be decreased to keep a constant computational effort proportional to $N_o^3 * N_{\text{at}}$.

We emphasize that, apart the use of a full electrons pseudo-potential at very high temperature, the **Extended method** is able to describe a whole isochore from zero temperature up to a few keVs within the same theoretical framework.

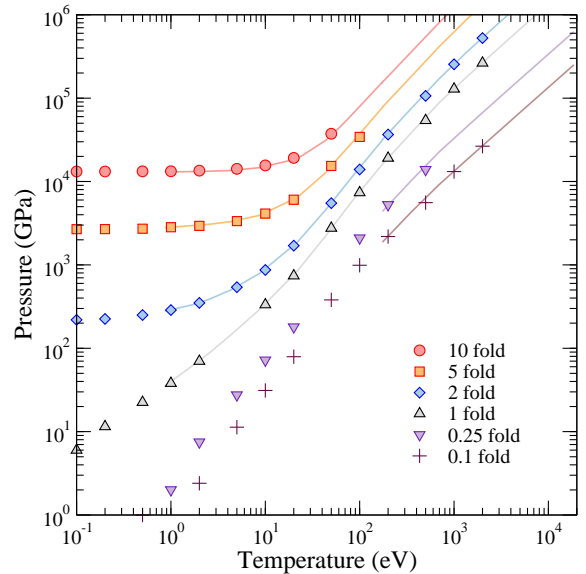


FIG. 7. **Extended method** aluminum x-fold compressed isochores (symbols) compared with Driver's data²¹ (solid lines).

In a forthcoming paper, we will give more details on the Hugoniot of aluminium in the very high temperature region characterized by oscillations.

VI. CONCLUSION

We have provided a quantitative estimation of the number of orbitals needed to reach a given level of precision at any temperature with a KSDFT calculation. We have shown that, for a fixed precision, this number increases dramatically with the temperature, banning the use of orbital based methods beyond a few tens of eVs. We have then implemented the Extended method in the ABINIT software package and shown how the introduction of the homogeneous electron gas density of states allows to correct poorly converged Kohn-Sham calculation with small number of orbitals, allowing to reach keVs temperatures straightforwardly.

ACKNOWLEDGMENTS

Vanina Recoules, Francois Soubiran and Burkhard Militzer are warmly acknowledged for stimulating discussions and for providing data and pseudo-potentials.

The data on aluminum isochore that support the findings of this study are available in the Supplemental of Driver's paper²¹, and other data are given in the Tables.

¹The ABINIT code is a common project of the Université Catholique de Louvain, Corning Incorporated, CEA and other contributors, (URL <http://www.abinit.org>).

²X. Gonze, B. Amadon, P.-M. Anglade, J.-M. Beuken, F. Bottin, P. Boulanger, F. Bruneval, D. Caliste, R. Caracas, M. Côté, et al., Computer Physics Communications **180**, 2582 (2009), ISSN 0010-4655, 40 YEARS OF CPC: A celebratory issue focused on quality software for high performance, grid and novel computing architectures, URL <http://www.sciencedirect.com/science/article/pii/S0010465509002276>.

³X. Gonze, B. Amadon, G. Antonius, F. Arnardi, L. Baguet, J.-M. Beuken, J. Bieder, F. Bottin, J. Bouchet, E. Bousquet, et al., Computer Physics Communications **248**, 107042 (2020), ISSN 0010-4655, URL <http://www.sciencedirect.com/science/article/pii/S0010465519303741>.

⁴G. Kresse and J. Furthmüller, Computational Materials Science **6**, 15 (1996), ISSN 0927-0256, URL <http://www.sciencedirect.com/science/article/pii/0927025696000080>.

⁵N. D. Mermin, Phys. Rev. **137**, A1441 (1965), URL <https://link.aps.org/doi/10.1103/PhysRev.137.A1441>.

⁶G. Kresse and J. Hafner, Phys. Rev. B **47**, 558 (1993), URL <https://link.aps.org/doi/10.1103/PhysRevB.47.558>.

⁷E. L. Pollock and D. M. Ceperley, Phys. Rev. B **30**, 2555 (1984), URL <https://link.aps.org/doi/10.1103/PhysRevB.30.2555>.

⁸S. Zhang, K. P. Driver, F. Soubiran, and B. Militzer, Phys. Rev. E **96**, 013204 (2017), URL <https://link.aps.org/doi/10.1103/PhysRevE.96.013204>.

⁹F. Lambert, J. Clérouin, S. Mazevet, and D. Gilles, Contributions to Plasma Physics **47**, 272 (2007), <https://onlinelibrary.wiley.com/doi/pdf/10.1002/ctpp.200710037>, URL <https://onlinelibrary.wiley.com/doi/abs/10.1002/ctpp.200710037>.

¹⁰F. Lambert, J. Clérouin, J.-F. Danel, L. Kazandjian, and S. Mazevet, *Properties of Hot and Dense Matter by Orbital-Free Molecular Dynamics* (World Scientific, Singapore, 2013), vol. 6 of *Recent Advances in Computational Chemistry*, pp. 165–201.

¹¹S. Mazevet, F. Lambert, F. Bottin, G. Zérah, and J. Clérouin, Phys. Rev. E **75**, 056404 (2007), URL <https://link.aps.org/doi/10.1103/PhysRevE.75.056404>.

¹²D. Sheppard, J. D. Kress, S. Crockett, L. A. Collins, and M. P. Desjarlais, Phys. Rev. E **90**, 063314 (2014), URL <http://link.aps.org/doi/10.1103/PhysRevE.90.063314>.

¹³J. F. Danel, L. Kazandjian, and G. Zérah, Physics of Plasmas **19**, 122712 (2012), URL <https://doi.org/10.1063/1.4773191>.

¹⁴S. Zhang, H. Wang, W. Kang, P. Zhang, and X. T. He, Physics of Plasmas **23**, 042707 (2016), <http://dx.doi.org/10.1063/1.4947212>, URL <http://dx.doi.org/10.1063/1.4947212>.

¹⁵J. Gaffney, S. Hu, P. Arnault, A. Becker, L. Benedict, T. Boehly, P. Celliers, D. Ceperley, O. Čertík, J. Clérouin, et al., High Energy Density Physics **28**, 7 (2018), ISSN 1574-1818, URL <http://www.sciencedirect.com/science/article/pii/S1574181818300508>.

¹⁶We count two electrons for one electronic state (G=2), also referred as orbital.

¹⁷F. Soubiran, F. González-Cataldo, K. P. Driver, S. Zhang, and B. Militzer, The Journal of Chemical Physics **151**, 214104 (2019), <https://doi.org/10.1063/1.5126624>, URL <https://doi.org/10.1063/1.5126624>.

¹⁸G. Chabrier and A. Y. Potekhin, Phys. Rev. E **58**, 4941 (1998), URL <https://link.aps.org/doi/10.1103/PhysRevE.58.4941>.

¹⁹V. Recoules, F. Lambert, A. Decoster, B. Canaud, and J. Clérouin, Phys. Rev. Lett. **102**, 075002 (2009), URL <http://link.aps.org/doi/10.1103/PhysRevLett.102.075002>.

²⁰F. Lambert, V. Recoules, A. Decoster, J. Clérouin, and M. Desjarlais, Physics of Plasmas **18**, 056306 (2011), URL <https://doi.org/10.1063/1.3574902>.

²¹K. P. Driver, F. Soubiran, and B. Militzer, Phys. Rev. E **97**, 063207 (2018), URL <https://link.aps.org/doi/10.1103/PhysRevE.97.063207>.

²²Private communication.

²³For high temperature calculations, some care in the evaluation of the DOS must be taken. The standard calculation using a broadening proportional to the temperature must be avoided, since it will wash out all the details. The DOS is here evaluated with a large number of k -points (770) and a small smearing value of 2 eV keeping a great level of details without any aliasing in the high energy range.

²⁴N. Holzwarth, A. Tackett, and G. Matthews, Computer Physics Communications **135**, 329 (2001), ISSN 0010-4655, URL <http://www.sciencedirect.com/science/article/pii/S0010465500002447>.